Quantitative acousto-optic imaging in tissue-mimicking phantoms

R. Molenaar*, A. Bratchenia, R.P.H. Kooyman
Faculty of Science and Technology, Institute of Biomedical Technology,
University of Twente
P.O. Box 217, 7500AE Enschede, the Netherlands

ABSTRACT

We have investigated the application of acousto-optic sensing for quantitative imaging of tissue-mimicking phantoms. An Intralipid phantom, which contains a turbid absorber, confined in a silicone tube, was used. Scattered pulsed laser light was modulated by ultrasonic bursts focused in a predefined volume in the medium. By varying the delay time between ultrasound burst initiation and light pulse firing we could perform a scan in the ultrasound-propagation plane. The use of calibration procedures allowed us to establish a quantitative correlation between local absorbances in the phantom and the measured signal and to obtain information on the ratios of dye concentrations inside the tube.

Keywords: quantitative imaging, acousto-optic spectroscopy, acousto-optic effect in turbid media

1. INTRODUCTION

The exploitation of optical methods to investigate certain aspects of human organs or tissue is an active research area. Their main advantages are that with relatively inexpensive instrumentation it is often possible to obtain local information without any invasive actions. In addition, moderate light intensities are harmless to tissue, as opposed to X-ray radiation. Unfortunately, light in the visible –near infrared region (λ~500-1500nm) is heavily scattered by tissue, which prevents penetration deep into tissue, and makes quantification of local optical properties, such as specific absorbances, difficult. Several approaches to circumvent this problem are under consideration. Particularly the combination of optics with ultrasound (US) appears attractive: because US is hardly scattered by tissue, its localization within tissue is much better defined than with an optical field. In the photo acoustic (PA) approach[1] a short intense laser pulse is applied to tissue. At positions where this light is absorbed a heat pulse and, consequently, a pressure pulse is generated. Owing to its nearly undisturbed propagation through tissue the origin of this pressure pulse can be very well localized using an acoustic transducer as detector. This approach is in a relatively advanced state of development, and is on its way to clinical use[2]. However, a quantitative interpretation of PA signals in terms of local absorbances, and thus of local concentrations of specific molecules, is difficult because these signals are dependent not only upon the local absorbance, but also on the local light fluences.
An alternative to PA is acousto-optics (AO): in this approach[3 4 5 6 7] light traveling through a certain region within a light-scattering structure can be acoustically labeled; this labeled light is optically detected outside the structure, and can relatively simple be interpreted in terms of local absorbances [8 9]. A spatial resolution of ~ 3 mm has been obtained.
In this paper we investigate the applicability of AO to the quantitative 3D mapping of absorbing structures in tissue-mimicking phantoms.

2. ACOUSTO-OPTICS AS AN IMAGING TOOL

AO in scattering media has its origin in two major types of interaction[10]: (1) a US field with frequency *f* induces in the structure under investigation (1) a periodic contraction/expansion of the medium resulting in a modulation with frequency *f* of the local refractive index; (2) a vibration with frequency *f* of scatter-particles present within the structure.

* r.molenaar@tnw.utwente.nl; phone +31534893053;

Medical Imaging 2009: Ultrasonic Imaging and Signal Processing, edited by Stephen A. McAleavey, Jan D'hooge
Proc. of SPIE Vol. 7265, 72650M · © 2009 SPIE · CCC code: 1605-7422/09/$18 · doi: 10.1117/12.814714

If simultaneously a light beam is sent through the structure the traversed light path will be modulated as a result of these material disturbances. Because the induced disturbances are rather small one has to rely upon interferometric methods to detect any modulation. Consequently, the use of a laser beam with good coherence properties is mandatory[11]; it turns out that detection of the time-dependent speckle pattern is an adequate means to analyze the US-induced disturbances.
Because a US field can be very well focused in tissue, the above-mentioned disturbances will have a well-defined localization within the structure, and only light that has traversed through this volume-element will undergo a pathlength modulation: this light has been pathlength-modulated labeled resulting in a speckle modulation on the detector. It will be clear that the light intensity within the US-disturbed volume is an important parameter determining the overall modulated speckle intensity; thus, the connection to a local absorbance of the disturbed volume-element is established.
In principle, by scanning the US-source over the structure of interest a map of local absorbances can be constructed; by using US *–pulses* in conjunction with laser pulses it is possible to label a relatively small volume-element [9], which for a US frequency of 2.25 MHz amounts to ~2*2*2 mm^3. This volume can be further decreased by using higher US-frequencies.

3. EXPERIMENTAL

3.1 The phantom

As a model system for an absorber-containing tissue we used a Perspex container (XYZ dimensions ~20x45x40 mm^3) filled with an Intralipid (IL) solution in an Agar matrix [12], with a reduced scattering coefficient μ_s'~1.95 mm^{-1}, i.e. similar to that in tissue. In the center of the phantom three silicone tubes were mounted perpendicularly to the X-axis (cf. fig. 1), with their axes along Y. Inner diameter of the tubes was 3 mm, their walls had a thickness of 0.5 mm. Their mutual wall-to-wall distance was ~5 mm. The tubes could be filled with IL/Agar mixed with an ink absorber of predefined absorbance. Each tube contained the same IL/agar/absorber mixture. This assembly can be considered as a simple model system for blood vessels embedded in tissue.

3.2 Acousto-optical setup

Consider Fig. 1. High pressure (~1.5 MPa) US bursts of ~ 1μs length, produced by an 2.25 MHz ultrasound transducer were sent along the Z-axis into the phantom. The focal point was chosen such that it coincided with the centers of the tubes. The employed US bursts resulted in an effective US disturbance volume of ~2x2x3 mm^3 around the focal point. The transducer was mounted on a computer-controlled XY translation stage with sub-mm resolution.
Light pulses of ~ 1μs duration, entering the phantom along the X-axis, were produced by deflection of a laser beam (514 nm, 260 mW) by an acousto-optic modulator. The delay time of this laser pulse relative to the start of the US burst could be set in the range 2-25 μs. The coherent light traveling through the phantom produced a speckle pattern that was detected by a CCD-camera (Basler A102f, 12 bits, 1380x1040 pixels). Using a 6 mm diaphragm the distance between container and camera was set such that approximately one speckle illuminated one pixel.

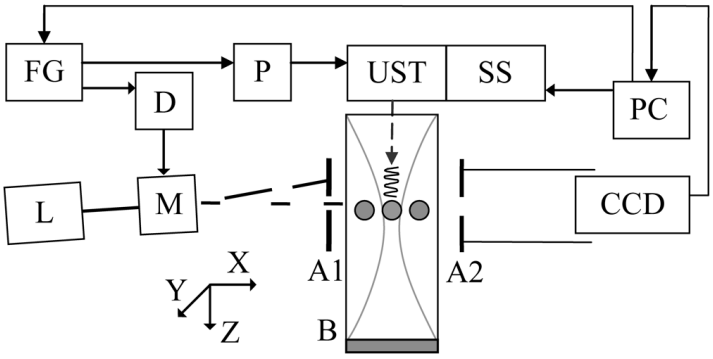

Fig. 1 Schematics of the acousto-optical setup in transmission geometry. FG: two-channel programmable function generator (Tektronix AFG3102). D: delay line. P: MOSFET pulser to drive transducer. UST: 2.25 MHz US transducer (Panametrics V306). SS: controllable scanning stage. L: Coherent Innova 70-Spectrum laser, 260 mW at 514 nm. M: acousto optical modulator (NeosTech 230803-LTD). A1: aperture to block non-deflected light. A2: aperture for speckle selection system. B: IL-based phantom. CCD: camera Basler A102f. In the center of the phantom the cross-section of an absorber containing tube is depicted. The US-propagation is along the Z direction.

3.3 Experiments

The delay time between laser pulse and acoustic pulse determined the Z-position of the phantom where the acoustic disturbance was measured. By varying this delay a Z-scan of the phantom could be made. An example of such a scan is depicted in fig. 2. By translating the US transducer in the XY-plane a 3D scan of the complete volume could be measured.

US – and laser pulses were applied at a rate of 30 kHz for a net camera exposure time of ~ 50 ms. The resulting image was processed as described in section 3.4. This setting resulted in a reasonable balance between on the one hand sufficient collected photons and on the other hand a limited influence of speckle decorrelation[9]. XYZ scans were done for the cases where the tubes were filled with absorbers with μ_a=0, 0.27, 0.54 mm^{-1}, respectively.

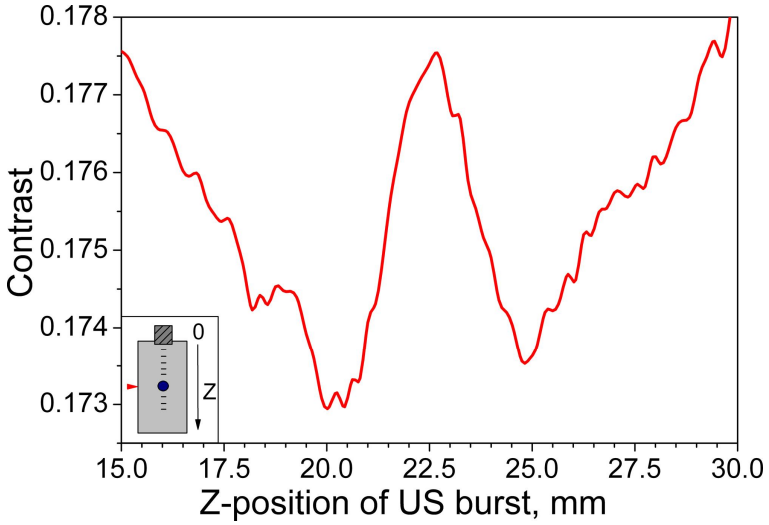

Fig. 2 Typical contrast profile C(z) through the sample. An absorber is present at $z \approx 22.5$ mm. The width of the absorber is ~3 mm. Contrast profile is spline interpolated.

3.4 Data treatment

An analysis of the camera's images is carried out by determining some statistical parameters of the speckle pattern[13] .The ultrasound disturbance induces a blurring of the speckles over the camera pixels. To quantify this effect, the speckle contrast C is introduced:

$$C = \frac{\sigma}{\mu} \tag{1}$$

Here, σ is the standard deviation of the pixel values of an image and μ is the mean pixel value. However, our main interest is in the relative change of C(z) when US is applied. To this end , we define the modulation depth:

$$M(z) = \frac{\Delta C(z)}{C(z)} \tag{2}$$

where $\Delta C = C_b - C$, C_b is the background contrast when no ultrasound is present and thus maximum contrast is measured. In our experiments, the modulation depth *M* can be used as a measure of the light fluence in the ultrasound volume. Fig.2 depicts a representative measurement of *C(z)*. It is seen that at the center of the strongly absorbing tube the contrast is a maximum, because within the tube there is hardly light present that can be US modulated. This figure gives also an impression of the vertical resolution that can be obtained: judging by the half width of the central peak a resolution of ~ 2 mm is found.

3.5 Calibration

Changes in *M* correspond only to absorber-caused changes of the fluence if the position of the UST and light source remain stationary; therefore a normalization procedure for *M* is appropriate that accounts for variations in the local fluence over the volume of the phantom. To this end we introduce the normalized modulation depth $\overline{M}$:

$$\overline{M}\left(\vec{r},\lambda\right)=\frac{M\left(\vec{r},\lambda\right)}{M_{\mu_a=0}\left(\vec{r},\lambda\right)} \tag{3}$$

Here, *M* is the modulation depth when an optical absorber is present in the US path. $M_{\mu a=0}$ is *M* measured in the absence of an optical absorber in the US path. $\vec{r}$ is the position of the center of the US modulation zone.

Because our aim is to interpret measured modulation depths in terms of local absorbances, we calibrated the instrument by measuring modulation depths as a function of known local absorbances . For the situation where one tube was filled with absorbers *M* was determined as function of μ_a , and the experimental data were fitted to a Lambert-Beer type model:

$$\overline{M}\left(\lambda\right)=\overline{M}_0\left(\lambda\right)*e^{-\Delta\mu_{ext}\left(\lambda\right)*l_{eff}\left(\lambda\right)}+\overline{M}_{bgd}\left(\lambda\right) \tag{4}$$

with l_{eff} the average of lightpath lengths through the US modulation zone, $\overline{M}_{bgd}$ is the normalized background modulation depth, mainly caused by residual US disturbances outside the absorbing region. $\Delta\mu_{ext}$ is the difference in extinction coefficient of the US-disturbed volume and its environment. In our phantom $\Delta\mu_{ext}=\Delta\mu_a$, because the scattering coefficient is constant over the whole phantom. Furthermore, $\overline{M}_0(\lambda)=(1-\overline{M}_{bgd})$.

For the employed wavelength (λ=514 nm) we found for the fitting coefficients $l_{eff}=(3.9\pm0.32)$mm, $\overline{M}_{bgd}=(0.16\pm0.02)$, determined for the range $0<\mu_a<1.5$ mm^{-1}.

4. RESULTS AND DISCUSSION

4.1 Normalized M vs. raw M

To investigate the effect of the introduction of $\overline{M}$ we have investigated to which extent the use of $\overline{M}$ enabled us to determine the absorption coefficient independent from the volume element position. By moving the US transducer along the X-axis a 2D map of *M*-values in the XZ-plane was determined, both for the situations where each tube contained no absorber and where an absorber was present. From these maps only those *M* corresponding to the Z-position of the vessels' centers were considered further.

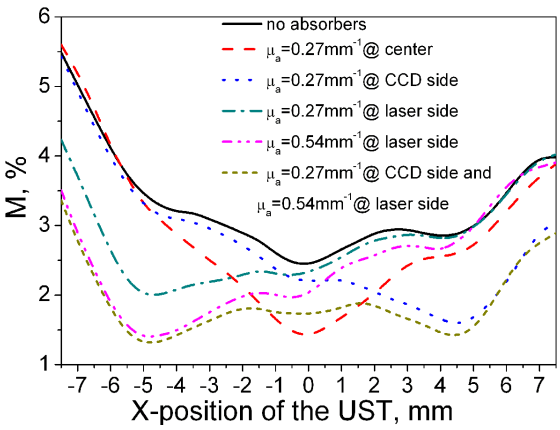

Fig. 3 (Color online) Measured modulation depth *M* as a function of the position of the US transducer in the three vessel phantom.

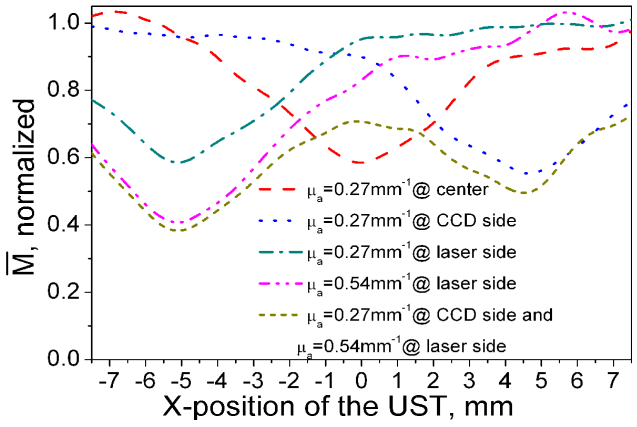

Fig. 4 (Color online) Measured normalized modulation depth as a function of the position of the US transducer in the three vessel phantom.

From a comparison of figs. 3 and 4 we see the effect of the conversion from M to $\overline{M}$: in Fig. 4 the application of the calibration data leads to different values for μ_a in the acousto-optically equivalent parts of the phantom. In Fig. 5, where $\overline{M}$ is depicted as a function of the transducer position, the variations in fluence are almost canceled out, resulting in a more reliable determination of the local μ_a.

These findings are corroborated by preliminary results from a numerical simulation of the AO experiment (figs 5 and 6), by solving the fluence diffusion equation for the phantom geometry under study. Particularly fig. 6, where $\overline{M}$ is depicted as a function of the transducer's position, shows a close resemblance to the experimental fig.4.

However, the normalization procedure is based on the assumption that anywhere in the phantom, except for the volume element which corresponds to the absorber confined in the US modulation zone, the fluence is the same both for the case of the phantom with absorber and phantom without absorbing inclusion. This assumption is less defendable for larger μ_a.

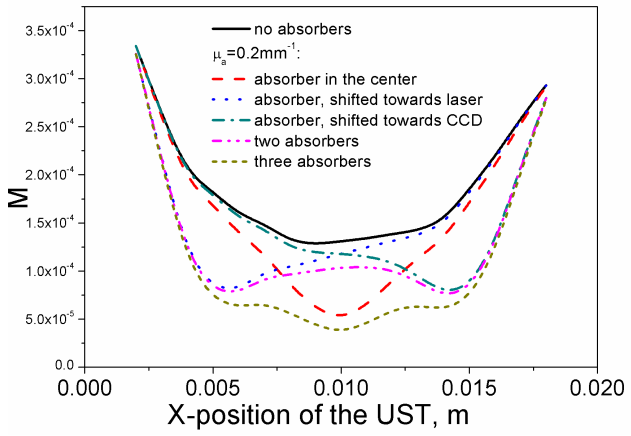

Fig. 5 (Color online) Calculated modulation depth M as a function of the position of the US transducer in the three vessel phantom. μ_a of absorbers was $0.2mm^{-1}$

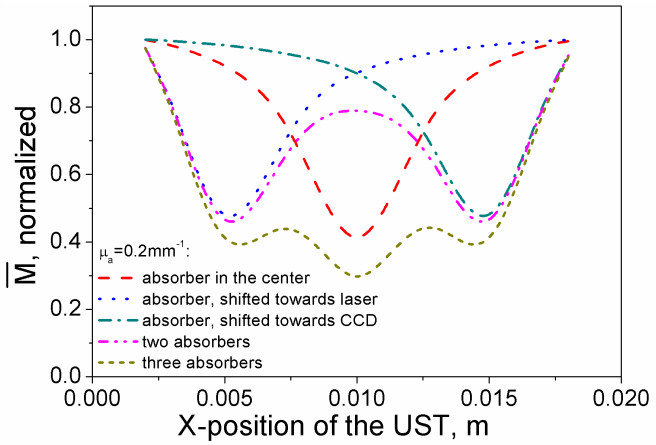

Fig. 6 (Color online) Calculated normalized modulation depth as a function of the position of the US transducer in the three vessel phantom. μ_a of absorbers was $0.2mm^{-1}$

4.2 Imaging

Subsequently, we have expanded the normalization approach to perform three-dimensional mapping of the phantom by moving the US transducer in the lateral XY plane. To demonstrate this, we built up *M*-value maps of the phantom, one for the phantom with the vessel filled with an absorbing scattering medium and another one for the phantom with the vessel which contains only the scattering medium. The cross-section of this map (along the X axis) is shown in Fig. 7, where *M*-maps are shown for both situations. Only a very close comparison of the two images reveals that in Fig. 7 an absorbing structure is present. However, by application of the normalization procedure, the presence of such a structure is obvious. Moreover, the application of the calibration data allows us to construct a local absorbance map, as shown in Fig. 8 for both one and two absorbing structures.

While for a single absorbing structure the μ_a-values given in fig. 8 appear quite accurate, it turns out that in the double-absorber structure (fig. 8b) this is less the case: it is seen that the two structures in fig 8b are depicted with somewhat different μ_a-values, although both absorbers were identically prepared. We expect that this limitation can be eliminated by the application of tomography methods, e.g. by rotating the light source and the detector around the objects of interest.

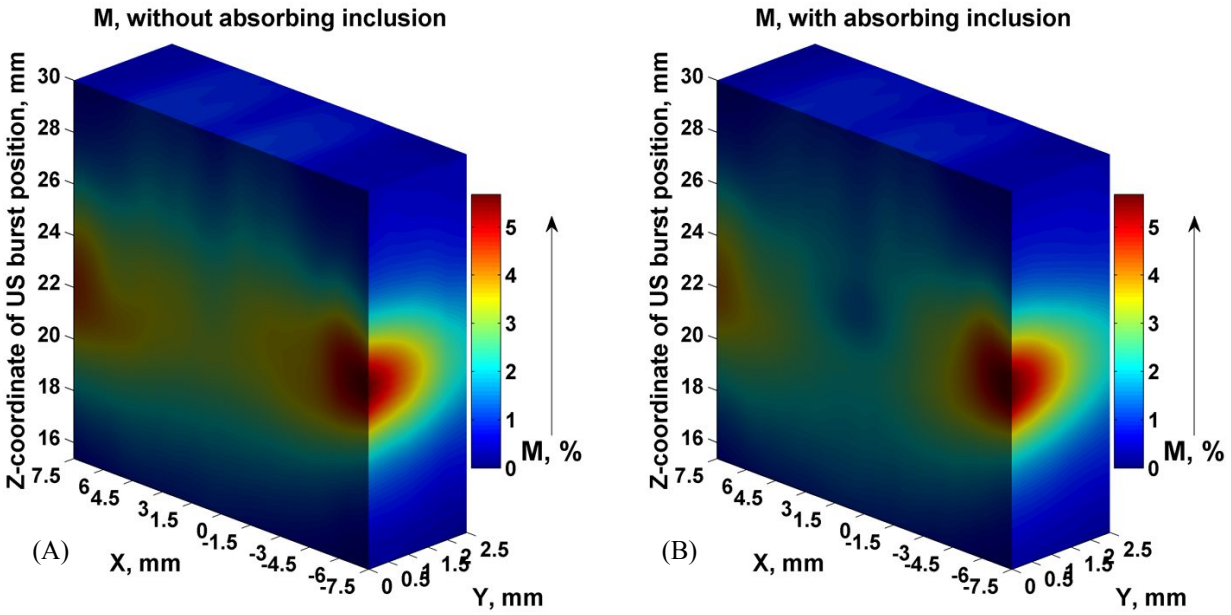

Fig. 7 The X axis cross-section of the map of M values. X, Y are the coordinates of the US transducer. Light is entering the phantom from the right. The central vessel within the phantom contains the absorbing dye. μ_a of absorber was $0.27mm^{-1}$ for λ= 514 nm.

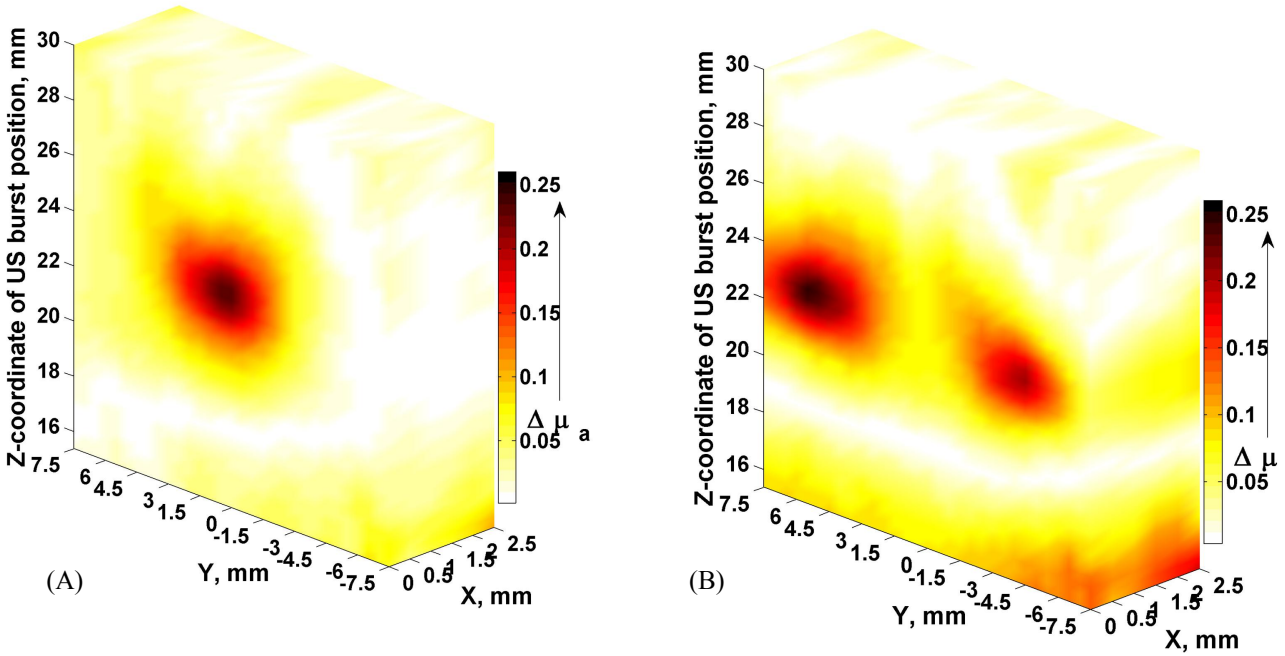

Fig. 8 The X axis cross-section of the map of $\Delta\mu_a \in [0;0.26]$ values of the three vessel phantom. X, Y are the coordinates of the US transducer. μ_a of absorbers was $0.27mm^{-1}$ for λ= 514 nm. Light is entering the phantom from the right. (a) The central vessel within the phantom contains the absorbing dye. (b) The outer vessels within the phantom contain the absorbing dye.

5. CONCLUSION

We have shown that Acousto-Optics can be used for quantitative three-dimensional mapping of tissue mimicking phantoms with a spatial resolution of about ~3mm. The used calibration technique allowed us to measure $\Delta\mu_a$ irrespective of the position of the absorber along the X axis. This technique can be extended to measurements of $\Delta\mu_a$ anywhere in a phantom, provided a map of $M_{\mu a=0}$ is available for the region of interest.
However, the normalization procedure, in which a set of measured modulation depth values M in the absence of absorbing inhomogeneities has to be measured, limits the application of the method to relatively homogeneous scattering media containing few absorbing inclusions. This limitation might be overcome by obtaining the baseline M numerically, e.g. by Monte-Carlo methods or by numerical solving the diffusion approximation for the radiative transfer equation.

6. ACKNOWLEDGMENTS

We thank Dr. P. Brands (ESAOTE) for help with the US instrumentation. This research was supported by the Technical Science Foundation of the Netherlands (STW) project TGT.6656.

7. REFERENCES

[1] X. Wang, Y. Pang, G. Ku, X. Xie, G. Stoica, and L.-H. V. Wang, "Non-invasive laser-induced photoacoustic tomography for structural and functional imaging of the brain in vivo", Nat. Biotechnol. 21, 803 (2003).
[2] S. Manohar, S. Vaartjes, J.C.G. Hespen, J.M. van, Klaase, F.M. van den Engh, W. Steenbergen & A.G.J.M. van Leeuwen, "Initial results of in vivo non-invasive cancer imaging in the human breast using near-infrared photoacoustics". Optics express, 15(19), 12277-12285 (2007).
[3] L.-H. Wang, S.L. Jacques, and X.-M. Zhao, "Continuous-wave ultrasonic modulation of scattered laser light to image objects in turbid media", Opt. Lett. 20, 629 (1995).
[4] W. Leutz and G. Maret, "Ultrasonic modulation of multiply scattered light", Physica B 204, 14 (1995)
[5] M. Kempe, M. Larionov, D. Zaslavski, and A.Z. Genack, "Acousto-optic tomography with multiply scattered light", J. Opt. Soc. Am. A 14, 1151 (1997).
[6] L.-H. V Wang, "Mechanisms of ultrasonic modulation of multiply scattered coherent light - an analytic model", Phys. Rev. Lett. 87, 043903 (2001).
[7] E. Granot, A. Lev, Z. Kotler, and B.G. Sfez, "Detection of inhomogeneities with ultrasound tagging of light", J. Opt. Soc. Am. A 18, 1962 (2001).
[8] C. Kim, R. J. Zemp, and L.-H. V. Wang, "Intense acoustic bursts as a signal-enhancement mechanism in ultrasound-modulated optical tomography," Opt. Lett. 31 (16), 2423-2425 (2006).
[9] A. Bratchenia, R. Molenaar, and R. P. H. Kooyman, "Feasibility of quantitative determination of local optical absorbances in tissue-mimicking phantoms using acousto-optic sensing," Appl. Phys. Lett. 92, 113901-(1-3) (2008).
[10] L-H. Wang, "Mechanisms of Ultrasonic Modulation of Multiply Scattered Coherent Light: An Analytic Model", Phys. Rev. Lett. 87, 043903 (2001).
[11] J. W. Goodman, "Statistical Properties of Laser Speckle Patterns," Chap.2 in Laser Speckle and Related Phenomena, J. C. Dainty ed., Springer-Verlag (1984).
[12] R. Cubeddu, A. Pifferi, P. Taroni, A. Torricelli and G. Valentini, "A solid tissue phantom for photon migration studies", Phys. Med. Biol. 42 , 1971 (1997).
[13] J. Li, G. Ku, L-H.Wang, "Ultrasound-modulated optical tomography of biological tissue by use of contrast of laser speckles", Appl Opt 41, 28 6030-6035 (2002).